Proceedings of the 3rd IASME/WSEAS Int. Conf. on FLUID DYNAMICS & AERODYNAMICS, Corfu, Greece, August 20-22, 2005 (pp118-123)

Secondary flows of shear-thinning generalized Newtonian fluids in curved pipes

NADIR ARADA
Instituto Superior Técnico
Dep. Matemática and CEMAT
Av. Rovisco Pais, 1049-001
Lisboa, PORTUGAL
anadir@math.ist.utl.pt

MARILIA PIRES
Universidade de Évora
Dep. Matemática and CIMA
Rua Romão Ramalho, 7000-671
Évora, PORTUGAL
marilia@uevora.pt

ADÉLIA SEQUEIRA
Instituto Superior Técnico
Dep. Matemática and CEMAT
Av. Rovisco Pais, 1049-001
Lisboa, PORTUGAL
adelia.sequeira@math.ist.utl.pt

(Dedicated to the memory of Professor Jindřich Nečas)

Abstract: - This paper presents a numerical study of the behavior of steady generalized Newtonian flows with shear-thinning viscosity in a curved pipe. Finite element simulations show in particular that, for sufficiently small curvature ratio and within a certain range of viscosity parameters, the secondary streamlines rotate and the flow field loses symmetry.

Key-Words: - curved pipe, finite elements, shear-thinning viscosity, wall shear stress, secondary flows.

1 Introduction

Steady fully developed viscous flows in curved pipes of circular, elliptical and annular cross-section of both Newtonian and non-Newtonian fluids, have been studied theoretically by several authors (see e.g. [9], [11], [13], [14], [15], [16], [17]) following the fundamental work of Dean ([7], [8]) for circular cross-section pipes. Using regular perturbation methods around the curvature ratio, Dean obtained analytical solutions in the case of Newtonian fluids. These results have been extended for a larger range of curvature ratio and Reynolds number, showing the existence of additional pairs of vortices and multiple solutions (see e.g. [18] and [6]).

Flows in curved pipes are considerably more complex than flows in straight pipes. In addition to the uniaxial flow, a secondary motion is driven outward due to centrifugal effects, forming a pair of symmetric vortices. This results in asymmetrical wall stresses with higher shear and low pressure regions (see e.g. [2], [16] and [12]).

The great interest in the study of curved pipe flows is due to its wide range of applications in engineering (e. g. hydraulic pipe systems related to corrosion failure) and in biofluid dynamics, such as blood flow in small size vessels where the viscosity shear-thinning behavior should not be neglected (see e. g. [4] and [5]). Numerical studies of velocity, pressure and wall shear stress distribution along the curved vessel may help to provide some understanding of the genesis of atherosclerosis and other arterial lesions (see e. g. [10] and references cited therein).

The aim of this paper is to present a numerical study of the behavior of steady fully developed flows of shear-thinning generalized Newtonian fluids in curved pipes with circular cross-section and arbitrary curvature ratio, for a prescribed pressure gradient. In particular, the numerical results show interesting shear-thinning viscosity effects: for sufficiently small curvature ratio and for certain viscosity parameter ranges, the flow field is quite complex, showing a rotation of the secondary streamlines and a loss of symmetry of the flow field. Stronger inertial effects seem to deform the pair of vortices and rotate the flow in an opposite direction.

These complex phenomena need to be further analyzed from the theoretical point of view. This will be the object of a forthcoming paper.

2 Governing equations

We consider steady isothermal flows of incompressible generalized Newtonian fluids with shear dependent viscosity (of Carreau-Yasuda type) in a curved pipe $\Omega \subset \mathbb{R}^3$ with boundary $\partial\Omega$. For these fluids, the extra-stress tensor is related to the kinematic variables through

$$\boldsymbol{\tau} = 2\left(\eta^* + \eta^{**}(1+|D\mathbf{u}|^2)^q\right) D\mathbf{u}, \qquad (1)$$

where $\mathbf{u}$ is the velocity field, $D\mathbf{u} = \frac{1}{2}(\nabla\mathbf{u} + \nabla\mathbf{u}^t)$ denotes the symmetric part of the velocity gradient, q is a real number, η^* and η^{**} are non-negative real numbers satisfying $\eta^* + \eta^{**} > 0$. The Cauchy stress tensor is given by $\mathbf{T} = -p\mathbf{I} + \boldsymbol{\tau}$, where p represents the pressure. The equations of conservation of momentum and mass hold in the domain Ω,

$$\rho\,\mathbf{u}\cdot\nabla\mathbf{u} + \nabla p = \nabla\cdot\boldsymbol{\tau}, \qquad \nabla\cdot\mathbf{u} = 0,$$

where $\rho > 0$ is the (constant) density of the fluid. We consider the dimensionless form of this system by introducing the following quantities

$$x = \frac{\widetilde{x}}{L}, \quad t = \frac{U\widetilde{t}}{L}, \quad u = \frac{\widetilde{u}}{U}, \quad p = \frac{\widetilde{p}L}{(\eta^*+\eta^{**})U},$$

where the symbol $\widetilde{\ }$ is attached to dimensional parameters (L represents a reference length and U a characteristic velocity of the flow). We also set $\eta = \frac{\eta^{**}}{\eta^*+\eta^{**}}$, and introduce the Reynolds number $\mathcal{R}e = \frac{\rho UL}{\eta^*+\eta^{**}}$. The dimensioneless system takes the form

$$\mathcal{R}e\,\mathbf{u}\cdot\nabla\mathbf{u} + \nabla p = \nabla\cdot\boldsymbol{\tau}, \quad \nabla\cdot\mathbf{u} = 0, \quad (2)$$

with adimensional extra stress tensor given by $\boldsymbol{\tau} = 2\big(1-\eta+\eta\big(1+|D\mathbf{u}|^2\big)^q\big)D\mathbf{u}$. This system is supplemented with a Dirichlet homogeneous boundary condition

$$\mathbf{u} = 0 \qquad \text{on } \partial\Omega. \quad (3)$$

3 Formulation in polar toroidal coordinates

Since we are concerned with steady flows in a curved pipe with circular cross-section, it is more convenient

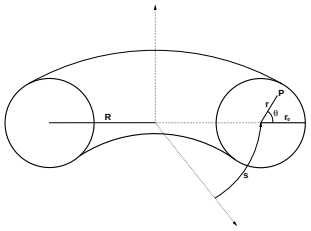

Figure 1: *A segment of curved pipe with centerline radius R and cross-sectional radius r_0.*

to use the polar toroidal coordinate system, in the variables $(\widetilde{r}, \widetilde{\theta}, \widetilde{s})$, defined with respect to the rectangular cartesian coordinates $(\widetilde{x}, \widetilde{y}, \widetilde{z})$ through the relations

$$\widetilde{x} = (R + \widetilde{r}\cos\theta)\cos\tfrac{\widetilde{s}}{R},$$

$$\widetilde{y} = (R + \widetilde{r}\cos\theta)\sin\tfrac{\widetilde{s}}{R}, \quad \widetilde{z} = \widetilde{r}\sin\theta,$$

with $0 < r_0 < R$, $0 \leqslant \widetilde{\theta} < 2\pi$ and $0 \leqslant \widetilde{s} < \pi R$. Introducing the axial variable and the pipe curvature ratio

$$s = \frac{\widetilde{s}}{r_0}, \qquad \delta = \frac{r_0}{R},$$

we see that the corresponding non-dimensional coordinate system is given by

$$x = \big(\tfrac{1}{\delta} + r\cos\theta\big)\cos(s\delta),$$

$$y = \big(\tfrac{1}{\delta} + r\cos\theta\big)\sin(s\delta), \qquad z = r\sin\theta,$$

with $\delta < 1$, $0 \leqslant \theta < 2\pi$ and $0 \leqslant s < \frac{\pi}{\delta}$. Let us now formulate problem (2) in this new coordinate system. To simplify the notation we set

$$\beta_1 = r\delta\sin\theta, \qquad \beta_2 \equiv \beta_2(r,\theta) = r\delta\cos\theta,$$

$$\beta \equiv \beta(r,\theta) = 1 + r\delta\cos\theta.$$

We consider fully developed flows. The components of the velocity are independent of the variable s, i.e.

$$\frac{\partial u}{\partial s} = \frac{\partial v}{\partial s} = \frac{\partial w}{\partial s} \equiv 0. \quad (4)$$

Consequently the axial component of the pressure gradient is a constant;

$$\frac{\partial p}{\partial s} = -p^*. \quad (5)$$

Taking into account (4)-(5) and using standard arguments, we rewrite problem (2) in the toroidal coordinates (r,θ,s). This problem is defined in the (bidimensional) set

$$\Sigma = \big\{(r,\theta) \in \mathbb{R}^2 \mid 0 < r < 1,\, 0 < \theta \leq 2\pi\big\},$$

and reads as follows

Find $(\mathbf{u} \equiv (u,v,w), p)$ solution of

$$\begin{cases} -\big(\nabla\cdot\boldsymbol{\tau} - \mathcal{R}e\,\mathbf{u}\otimes\mathbf{u}\big)_r + \frac{\partial p}{\partial r} = 0, \\ -\big(\nabla\cdot\boldsymbol{\tau} - \mathcal{R}e\,\mathbf{u}\otimes\mathbf{u}\big)_\theta + \frac{1}{r}\frac{\partial p}{\partial\theta} = 0, \\ -\big(\nabla\cdot\boldsymbol{\tau} - \mathcal{R}e\,\mathbf{u}\otimes\mathbf{u}\big)_s + \frac{p^*}{\beta} = 0, \\ \frac{\partial}{\partial r}(r\beta u) + \frac{\partial}{\partial\theta}(\beta v) = 0, \\ \mathbf{u}_{|\partial\Omega} = 0, \end{cases} \quad (6)$$

where

$$\nabla \mathbf{u} = \begin{pmatrix} \frac{\partial u}{\partial r} & \frac{\partial v}{\partial r} & \frac{\partial w}{\partial r} \\ \frac{1}{r}\frac{\partial u}{\partial \theta} - \frac{v}{r} & \frac{1}{r}\frac{\partial v}{\partial \theta} + \frac{u}{r} & \frac{1}{r}\frac{\partial w}{\partial \theta} \\ -\frac{\beta_2}{r\beta} w & \frac{\beta_1}{r\beta} w & \frac{\beta_2}{r\beta} u - \frac{\beta_1}{r\beta} v \end{pmatrix},$$

and where $\nabla \cdot \boldsymbol{\sigma}$ is given by

$$\begin{aligned} r\beta\left(\nabla\cdot\boldsymbol{\sigma}\right)_r &= \frac{\partial}{\partial r}\left(r\beta\boldsymbol{\sigma}_{rr}\right) + \frac{\partial}{\partial\theta}\left(\beta\boldsymbol{\sigma}_{r\theta}\right) + \frac{\partial}{\partial s}\left(r\boldsymbol{\sigma}_{rs}\right) \\ &\quad -\beta_2\boldsymbol{\sigma}_{ss} - \beta\boldsymbol{\sigma}_{\theta\theta}, \\ r\beta\left(\nabla\cdot\boldsymbol{\sigma}\right)_\theta &= \frac{\partial}{\partial r}\left(r\beta\boldsymbol{\sigma}_{\theta r}\right) + \frac{\partial}{\partial\theta}\left(\beta\boldsymbol{\sigma}_{\theta\theta}\right) + \frac{\partial}{\partial s}\left(r\boldsymbol{\sigma}_{\theta s}\right) \\ &\quad +\beta_1\boldsymbol{\sigma}_{ss} + \beta\boldsymbol{\sigma}_{r\theta}, \\ r\beta\left(\nabla\cdot\boldsymbol{\sigma}\right)_s &= \frac{\partial}{\partial r}\left(r\beta\boldsymbol{\sigma}_{sr}\right) + \frac{\partial}{\partial\theta}\left(\beta\boldsymbol{\sigma}_{s\theta}\right) + \frac{\partial}{\partial s}\left(r\boldsymbol{\sigma}_{ss}\right) \\ &\quad -\beta_1\boldsymbol{\sigma}_{\theta s} + \beta_2\boldsymbol{\sigma}_{rs}. \end{aligned}$$

4 Numerical approximation

Finite element methods are used to obtain approximate solutions to system (6). The algorithm we consider to solve the problem is based on Newton's method, the non-linear part being explicitely calculated at each iteration step. In order to study the effect of the non-constant viscosity, we compare the qualitative behavior of the axial velocity, the stream function and the wall shear stress of both Newtonian and generalized Newtonian fluids. Calculations were achieved for different values of the parameters involved in the governing equations (the Reynolds number $\mathcal{R}e$, the curvature ratio δ, the non-dimensional viscosity parameter η and the exponent q appearing in the power-law type viscosity). A continuation method is carried out to implement these different tests.

When the Reynolds number is set to zero (creeping flows), there is no secondary motion and no wall shear stress and as expected, the solution is of Poiseuille type in both cases. The contours of the axial velocity w are circles, centered about the central axis in the case of a small curvature and are shifted away from the center when δ increases. The only difference between the Newtonian and generalized Newtonian flows is related to the maximal value achieved by w, which increases with $|q|$, before stabilizing for some value of this parameter.

4.1 Inertial Newtonian flows

If $\mathcal{R}e \neq 0$, it is well known that a "slight curvature" of the pipe axis induces centrifugal forces on the fluid which forms a secondary flow. A pair of symmetric vortices is then superposed to the axial Poiseuille flow,

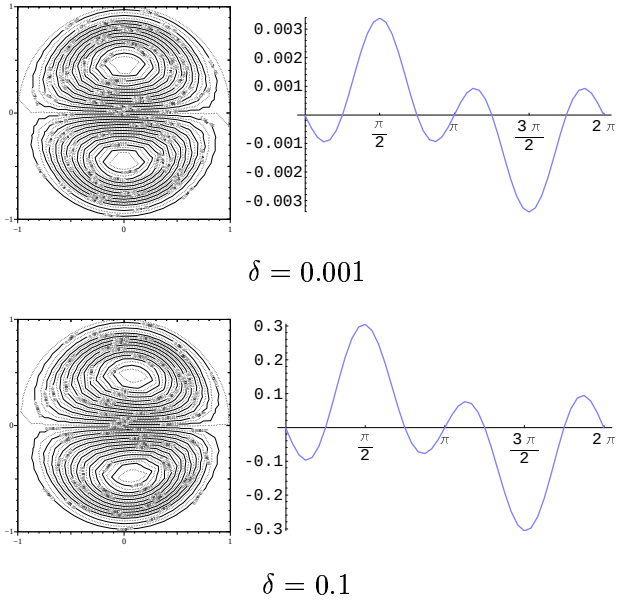

Figure 2: *Streamlines and wall shear stress for Newtonian flows* ($\mathcal{R}e = 70$).

and strengthen when $\mathcal{R}e$ increases. The effect of the curvature ratio is similar to the case of creeping flows. In Figures 2, we plot the contours of the stream function and the wall shear stress for $\mathcal{R}e$=70, δ=0.001, and δ=0.1. As can be observed, the contours of the stream function show a shift from the center in the last case. The behavior of the wall shear stress is identical. The only difference is related to the amplitude which clearly depends on the Reynolds number and on the curvature ratio.

4.2 Shear-thinning flows

Inertial generalized Newtonian flows are more complex. The contours of the stream function, as well as the wall shear stress vary with respect to the parameters η and q, appearing in the definition of the viscosity function, and with respect to the Reynolds $\mathcal{R}e$. Because of the highly non-linear nature of the model, the interaction between the corresponding terms, namely the convective and the viscosity terms, is difficult to handle.

We first consider the case of a "slightly curved" pipe (δ=0.001). Fixing $\mathcal{R}e$, we increase the parameter η (together with $|q|$) in order to study the effect of the viscosity. As can be seen in Tables 2-3, the flow seems to behave in three different ways, depending on the value of the viscosity parameter, namely for η taking values in the sub-intervals $[0,\ 0.4[$, $[0.4,\ 0.6[$ and $[0.6,\ 1[$.

Table 1 shows the maximum value $q_{\max}$ obtained for

each one of the cases considered. For a fixed η, we have globally the same range of values, independently of the Reynolds number. For $\eta \in [0,\ 0.4[$, $q_{\max}$ is a constant. For $\eta = 0.4$ and $\eta = 0.5$, the maximum value increases with $\mathcal{R}e$, while it decreases for η taking the values 0.6, 0.7 and 0.9. As we shall see below,

η		0.1	0.2	0.4	0.5	0.6	0.7	0.9
$\mathcal{R}e$	1	72.5	72.5	6.7	5.0	3.4	1.8	0.6
	15	72.5	72.5	25.2	5.9	2.9	1.7	0.6
	30	72.5	72.5	24.3	5.9	2.5	1.4	0.6
	50	72.5	72.5	28.3	5.9	2.4	1.2	0.6
	70	72.5	72.5	31.6	5.8	2.1	1.2	0.5

Table 1: *Maximum values for* $|q|$.

one of the surprising effects of the non-constant viscosity on the secondary flows, verifiable at least for small curvature ratios, is the rotation of the contours. Table 2 deals with the global behavior of these contours for different values of the parameters. Notation S and L refer respectively to symmetric and left-rotating contours, while L-S refers to contours that rotate to the left and then to the right, before stabilizing in a symmetric way.

η		0.1	0.2	0.4	0.5	0.6	0.7	0.9
$\mathcal{R}e$	1	S	L-S	L	L	L	S	S
	15	S	L-S	L-S	L	L	S	S
	30	S	L-S	L-S	L	S	S	S
	50	S	L-S	L-S	S	S	S	S
	70	S	L-S	L-S	S	S	S	S

Table 2: *Qualitative behavior of the contours.*

η		0.1	0.2	0.4	0.5	0.6	0.7	0.9
$\mathcal{R}e$	1	–	19	6.0	4.0	2.9	–	–
	15	–	19	6.0	4.0	2.8	–	–
	30	–	19	6.0	4.2	–	–	–
	50	–	19	6.0	–	–	–	–
	70	–	19	6.0	–	–	–	–

Table 3: *Values for* $|q_{var}|$ *initiating the rotation.*

Table 3 presents the values of $|q_{var}|$ corresponding to the viscosity exponent that initiates the rotation (when it occurs). It is clear that q_{var} decreases as η increases. Moreover, for η fixed, this exponent is constant and independent of the values of the Reynolds number.

For η=0.1, the contours are still symmetric and the qualitative behavior is of Newtonian type. The only difference lies in the values of the stream function, which increase in absolute value with the exponent q and with $\mathcal{R}e$, while the axial velocity is constant.

For η=0.2 (respectively η=0.3 and 0.4), interesting phenomena can be observed. Initially, the behavior is identical to the previous case, but as $|q|$ increases, we observe a variation in the shape of the vortices, their displacement to the core, the concentration of the contours and the reduction of the global surface in this region. For $q \equiv q_{var}$=-19 (respectively q_{var}=-9 and q_{var}=-6), the contours initiate a counter-clockwise rotation, augmenting with $|q|$. At some level, a stabilization can be noticed, followed by a clockwise rotation where the inverse phenomenon occurs: weakening of the contours in the core region, distancement of the vortices and decreasing of the angle of rotation till the recovery of the symmetry (see Figures 3-4). Let us also observe that even if the rotation initiates at the same exponent independently of the Reynolds number, the inertial forces seem to oppose resistance and clearly affect the maximum angle of rotation.

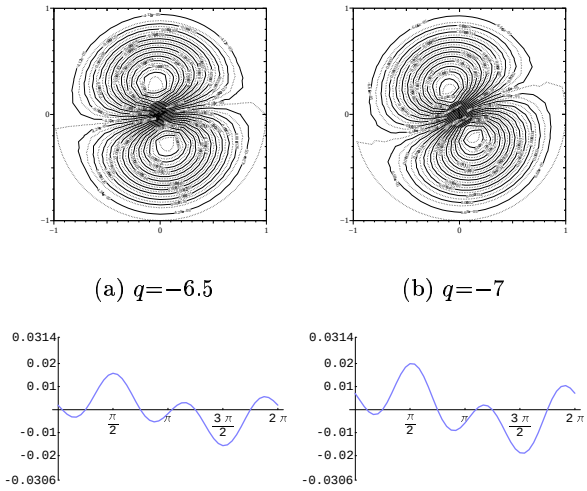

(a) q=-6.5 (b) q=-7

(c) q=-6.5 (d) q=-7

Figure 3: *Streamlines and wall shear stress for* $\mathcal{R}e$=30 *and* η=0.4.

Parallel variations in the behavior of the wall shear stress can be observed. Initially, the behavior is of Newtonian type, with symmetries relatively to the horizontal axis and to the vertical axis θ=π, and with the wall shear stress vanishing at θ=0, π and 2π. Some modifications can be observed when the viscosity exponent reaches q_{var}, and are more visible for relatively small values of $\mathcal{R}e$. At this level, there is lost of symmetry with respect to both axis and the wall shear stress takes positive values at θ=0, 2π and negative values at θ=π. As $|q|$ increases, there is a stabilization with recovering of the symmetry but for a different

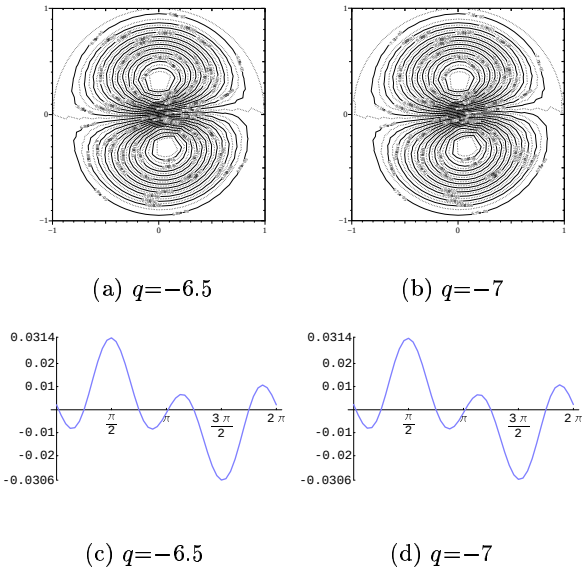

(a) q=−6.5 (b) q=−7

(c) q=−6.5 (d) q=−7

Figure 4: *Streamlines and wall shear stress for* $\mathcal{R}e$=70 *and* η=0.4.

type of curve. Finally, the inverse behavior initiates until we recover the original state.

Let us also observe that for a fixed η, the behavior of the maximum values for the axial velocity is independent of $\mathcal{R}e$ and that it increases in absolute value with respect to $|q|$, while the maximum values of the stream function increases with $\mathcal{R}e$ and, for a fixed viscosity parameter, have the same behavior as the contours: they first increase, they stabilize and finally decrease.

The case $\eta = 0.5$ is particular in the sense that it represents a limit for the behavior of the flow. For $\mathcal{R}e$=15 and $\mathcal{R}e$=30, the case is similar to the previous ones. However, at least for the achieved tests, no clockwise rotations have been observed. This fact together with the shape of the vortices and the strong deformation of the contours in their neighborhood suggest that we are in the presence of some "forces" in opposition to the rotation. This can be confirmed when considering the case of $\mathcal{R}e$=70, where the vortices shift away from the center and where the streamlines initiate a slight clockwise slope. Finally, the cases corresponding to $\eta \geq 0.6$ are more stable. Even if the maximum value of $|q|$ achieved is relatively small, which limits our conclusions, a careful analysis of the different plots show that the opposition to the rotation is stronger in these cases.

Next we consider the behavior of the stream function and of the wall shear stress for an intermediate curvature ratio. The idea is basically to compare with the case studied in the last section, and to analyze the effect of the curvature on the observed phenomenon. As previously, we made several tests involving different Reynolds numbers, different viscosity parameters and implementing a continuation method for the viscosity exponent q.

In contrast to the previous case, one of the direct conclusions when analyzing the results corresponding to the intermediate curvature ratio is the fact that the behavior of the flow is much more stable (see Tables 4 -5 and Figure 5).

η		0.4	0.5	0.6	0.7	0.9
$\mathcal{R}e$	1	36.7	4.5	2.10	1.30	0.59
	15	7.25	3.05	1.60	0.70	0.42
	30	7.15	2.95	1.20	0.70	0.36
	50	3.80	1.85	0.75	0.55	0.34
	70	0.62	0.46	0.34	0.28	0.20

Table 4: *Maximum values for the exponent* $|q|$.

η		0.4	0.5	0.6	0.7	0.9
$\mathcal{R}e$	1	S	L-S	S	S	S
	15	S	S	S	S	S
	30	S	S	S	S	S
	50	S	S	S	S	S
	70	S	S	S	S	S

Table 5: *Qualitative behavior of the contours.*

Indeed, we did not observe any rotation and the contours of the stream function remain symmetric. The only remarkable fact is related to variations in the shape of the vortices and their shift from the center. This behavior initiates for small values of the viscosity exponent $|q|$, and is more pronounced when $\mathcal{R}e$ increases.

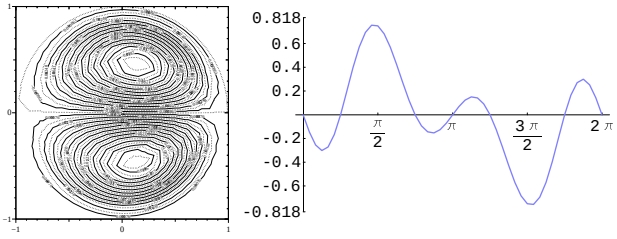

Figure 5: *Streamlines and wall shear stress for* $\mathcal{R}e$=70 *and* η=0.4 *and* q=−0.6.

The maximum values for the stream function increase with $|q|$, with η and with $\mathcal{R}e$. The same observation can be done for the axial velocity which, contrarily to the case of small curvature ratio, is sensitive to the variations of $\mathcal{R}e$. This stability can also be observed in

the behavior of the wall shear stress. The corresponding curves are of Newtonian type (with symmetries relatively to the axis) and amplitude (for a fixed η and a fixed $\mathcal{R}e$) increases with $|q|$. However, in contrast to the Newtonian type, for a fixed q and a fixed η, the amplitude of the wall shear stress decreases when the Reynolds number increases.

5 Conclusion

A two-dimensional finite element code has been developed for the simulation of generalized Newtonian fluids with shear-thinning viscosity presented in this paper. Attention is focused on steady fully developed flows in curved pipes of circular cross-section. The axial pressure gradient is specified and parametric studies involving the symmetry of the streamline contours of secondary flows and the wall shear stress are performed for certain curvature ratios, to analyze the corresponding inertial and viscosity effects as a function of the Reynolds number and the viscosity parameters (viscosity ratio and power-index).

A more detailed discussion on the complex behavior of these flows is done in [1] and can also be found in [13] where Oldroyd-B flows with shear-dependent viscosity are considered and viscoelasticity effects are also taken into account.

Future work will be mainly directed to the numerical study of pulsatile flows in view of its application to blood flow in curved vessels where the distribution of velocities, pressure and wall shear stresses may help to provide some understanding of the genesis of atherosclerosis and other arterial lesions.

Acknowledgements: This work has been partially supported by the grant SFRH/BPD/3506/2000 of Fundação para a Ciência e a Tecnologia (N. Arada), by the Center for Mathematics and its Applications (CEMAT) through FCT's Funding Program, and the Projects POCTI/MAT/41898/2001 and HPRN-CT-2002-00270.

References:

[1] N. Arada, M. Pires and A. Sequeira, Viscosity effects on flows of generalized Newtonian fluids through curved pipes, Computers and Mathematics with Applications, 2005, accepted for publication.

[2] S. A. Berger, L. Talbot and L.-S. Yao, Flow in curved pipes, Ann. Rev. Fluid Mech., 15, 461-512, 1983.

[3] W. Y. Soh and S. A. Berger, Fully developed flow in a curved pipe of arbitrary curvature ratio, Int. J. Numer. Meth. Fluid., 7, 733-755, 1987.

[4] S. Chien, S. Usami, R. J. Dellemback, M. I. Gregersen, Blood viscosity: influence of erythrocyte deformation, Science 157 (3790), 827-829, 1967.

[5] S. Chien, S. Usami, R. J. Dellemback, M. I. Gregersen, Blood viscosity: influence of erythrocyte agragation, Science 157 (3790), 829-831, 1967.

[6] P. Daskopoulos and A. M. Lenhoff, Flow in curved ducts: bifurcation structure for stationary ducts, J. Fluid Mech., 203, 125-148, 1989.

[7] W. R. Dean, Note on the motion of fluid in curved pipe, Philos. Mag., 20, 208, 1927.

[8] W. R. Dean, The streamline motion of fluid in curved pipe, Philos. Mag., 30, 673, 1928.

[9] Y. Fan, R. I. Tanner and N. Phan-Thien, Fully developed viscous and viscoelastic flows in curved pipes, J. Fluid Mech., 440, 327-357, 2001.

[10] F. J. H. Gijsen, E. Allanic, F. N. van de Vosse, J. D. Janssen, The influence of the non-Newtonian properties of blood on the flow in large arteries: unsteady flow in a 90^o curved tube, Journal of Biomechanics, 32, 705-713, 1999.

[11] H. Ito, Flow in curved pipes, JSME Int. J., 30, 543-552, 1987.

[12] T. J. Pedley, *Fluid mechanics of large blood vessels*, Cambridge University Press, Cambridge (1980).

[13] M. Pires, *Mathematical and numerical analysis of non-Newtonian fluids in curved pipes*, PhD thesis, IST, Lisbon (2005).

[14] A. M. Robertson, On viscous flow in curved pipes of non-uniform tion, Inter. J. Numer. Meth. fluid., 22, 771-798, 1996.

[15] A. M. Robertson and S. J. Muller , Flow of Oldroyd-B fluids in curved pipes of circular and annular cross-section, Int. J. Non-Linear Mechanics, 31, 1-20, 1996

[16] W. Y. Soh and S. A. Berger, Fully developed flow in a curved pipe of arbitrary curvature ratio, Int. J. Numer. Meth. Fluids, 7, 733-755, 1987.

[17] H. C. Topakoglu and M. A. Ebadian, On the steady laminar flow of an incompressible viscous fluid in a curved pipe of elliptical cross-section, J. Fluid Mech., 158, 329-340, 1985.

[18] Z. H. Yang and H. B. Keller, Multiple laminar flows through curved pipes, Appl. Numer. Math., 2, 257-271, 1986.